Direct *ab initio* dynamics studies of vibrational-state selected reaction rate of the $OH+H_2 \rightarrow H+H_2O$ reaction

Thanh N. Truong
Department of Chemistry, University of Utah, Salt Lake City, Utah 84112

(Received 14 November 1994; accepted 19 December 1994)

We present direct *ab initio* dynamics studies of vibrational-state selected reaction rates of the $OH+H_2 \rightarrow H+H_2O$ reaction. Rate constants for both the $OH+H_2(v=1)$ and $OH(v=1)+H_2$ reactions were calculated based on a full variational transition state theory plus multidimensional semiclassical tunneling approximations within a statistical diabatic model. The potential energy surface information was calculated at an accurate level of molecular orbital theory. In particular, geometries and frequencies along the minimum energy path were calculated at the quadratic configuration interaction level including all single and double excitations (QCISD) with the 6-311+G(d,p) basis set. Energies along the minimum energy path were further improved by a series of single point projected fourth-order Möller–Plesset perturbation theory (PMP4) calculations using the 6-311++G($2df,2pd$) basis set. Our present results of vibrational excited state rate enhancements agree very well with previous experimental data. In view of these results, we also discuss the accuracy of the Schatz–Elgersma potential energy function in more detail. © *1995 American Institute of Physics.*

I. INTRODUCTION

Effects of reagent energies on the reaction rate of bimolecular reactions have been a focus of many theoretical and experimental studies. In particular, the

$$OH(v)+H_2(v') \rightarrow H+H_2O \qquad \text{(R1)}$$

reaction is emerging as a benchmark reaction for theoretical studying of the effect of reagent vibrational energy on reactivity of elementary gas phase reactions.[1–15] This is because (i) the $OH+H_2$ reaction is an important process in combustion chemistry, (ii) its small size permits accurate quantum scattering calculations to be carried out,[6,11,12] (iii) there exists a reasonably accurate *ab initio* potential energy function (PEF), denoted as Schatz–Elgersma (SE) PEF,[4] for this reaction, and (iv) experimental thermal rate constants,[16–23] kinetic isotope effects,[18] and rate constants for vibrational excitations of either reactant are available.[24,25] In fact, it has been known experimentally that OH vibrational excitation has a negligible effect on the rate of reaction (R1)[26] whereas H_2 vibrational excitation was found to enhance the rate by a factor of 120 ± 40 by Zellner and Steiner,[25] and a factor of 155 ± 38 by Glass and Chaturvedi[24] at 298 K. Theoretical studies of the vibrational mode specific rate enhancements so far have some mixed success. All previous theoretical studies correctly predicted the small rate enhancement due to the excitation of the OH stretch.[5,9–11] However, results for the rate enhancement factor due to the H_2 excitation varied widely[1,5,9–12] and are not in quantitative agreement with experiments even from recently full 6D quantum scattering calculations,[11,12] which are considered as the most extensive calculations to date. Although these two full quantum calculations[11,12] are in quantitative agreements with each other, the predicted rate enhancement factor for exciting the H_2 vibration of 805 at 300 K is too large.[11] The authors[11] attributed this large factor to the resonance-like peaks at low kinetic energies observed in the calculated reaction probability for the $OH(v=0)+H_2(v'=1)$ reaction. Such peaks were thought to be due to the unphysical well in the entrance channel, even though this well had been mostly removed in the employed modified SE PEF.[11] Removing these resonance peaks still yields the enhancement factor of 388. A less accurate 3D quantum scattering study,[1] which were based on a rotating bond approximation, yielded excellent agreement with experimental data on the enhancement factor. However, in view of the full dimensional quantum calculations, such agreements may require further investigation. Previous quasiclassical (QC) trajectory calculations predicted the enhancement factor of 393.[10] Using the original SE PEF, variational transition state theory plus multidimensional tunneling corrections calculations based on a diabatic model for the $OH+H_2(v'=1)$ reaction noticeably underestimated the enhancement factor, a factor of 27 at 298 K.[9] In addition, full quantum rate calculations predicted thermal rate constants too large particularly at low temperatures.[6] Such poor agreements with experimental observations have been attributed to defects in the analytical Schatz–Elgersma PEF.

In our previous direct *ab initio* dynamics study of the $H+H_2O \leftrightarrow OH+H_2$ reaction,[27] we found that the PMP4/6-311++G($2df,2pd$)//QCISD/6-311+G(d,p) level of theory can provide accurate potential energy information for dynamical calculations. In this case, geometries and frequencies along the minimum energy path were calculated at the QCISD/6-311+G(d,p) level whereas energetic information was further improved by a series of single point PMP4/6-311++G($2df,2pd$) calculations. Our calculated thermal rate constants for both the forward and reverse reactions of (R1) agree very well with experimental data for a wide range of temperature.

In this study, our objectives are twofold. One is to study the vibrational mode specific rate enhancement in the $OH+H_2$ reaction using our direct *ab initio* dynamics approach as described earlier, and particularly to examine the validity of the diabatic approximation in calculating

vibrational-state selected rate constants. The other is to investigate the accuracy of the SE PEF particularly in the entrance channel of the $OH+H_2$ reaction. It is important to point out that our present study can only test the accuracy of the SE PEF along the reaction valley which is the most important region for the dynamics of this reaction. This study would not be able to identify errors in other regions of the global SE PEF. Our present calculations were based on a full variational transition state theory (VTST) including multidimensional tunneling corrections within a vibrationally adiabatic model. We also have performed the same VTST calculations but with the Schatz–Elgersma PEF. This would allow us to discuss how defects in the analytical SE PEF manifests in the calculated vibrational-state selected rates of the $OH+H_2$ reaction.

II. THEORY

The statistical diabatic model to be used with a variational transition state theory plus multidimensional tunneling correction for calculating vibrational-state selected rate constants for the $OH(v)+H_2(v')$ reaction has been presented earlier,[9] thus it is only briefly discussed here. For reaction (R1), there are a total of five generalized vibrational modes, namely, the two out-of-plane bending modes having a'' symmetry, and the stretching and in-plane bending modes having a' symmetry. Within the reaction-path Hamiltonian formalism, modes with the same symmetry cannot cross. It has been pointed out by Truhlar and Isaacson[9] that a better approximation would be to assume that vibrational modes preserve their characteristics along the reaction coordinate. This can be accomplished by correlating vibrational modes by maximizing the overlaps between two successive points along the reaction coordinate.

Vibrational-state selected canonical variational transition state theory (CVT) rate constants at the temperature T were then determined by minimizing the vibrational-state selected generalized transition state theory (GTST) rate constants with respect to the location of the dividing surface that is orthogonal and intersects the reaction coordinate at the value s. Within the statistical-diabatic model, the vibrational-state selected rate constants differ from the statistical form for the thermal rate only in the vibrational partition function for the selected mode. In particular, the vibrational partition of mode i in state m is given by

$$q_i(m,T)=e^{-(1/2+m)\hbar w_i/kT}, \tag{1}$$

where k is the Boltzmann constant. In CVT rate, the motion along the reaction coordinate is still treated classically. Tunneling along this degree of freedom is included by a transmission coefficient. In this study, the effective (diabatic) potential for tunneling in the vibrational-state selected reaction is defined by

$$V_d(\{m_i\},s)=V_{\mathrm{MEP}}(s)+\sum_{i=1}^{3N-7}\left(\frac{1}{2}+m_i\right)\hbar w_i(s), \tag{2}$$

where m_i is the vibrational state of mode i and $3N-7$ is the number of generalized frequencies for the nonlinear N-atom polyatomic system. In Eq. (2), modes that do not correlate to the reactant vibrations in particular selected states are assumed to be in the ground state. The transmission coefficients were calculated with the multidimensional semiclassical tunneling methods described elsewhere. In this study, both the zero-curvature tunneling (ZCT) and small-curvature tunneling (SCT) methods were employed. The SCT transmission coefficients, that include the reaction-path curvature effect on the transmission probability, were based on the centrifugal-dominant small curvature semiclassical adiabatic ground-state CD-SCSAG approximation[28] with modifications for the vibrational-state selected case. In particular, the transmission probability at energy E is given by

$$P(E)=\frac{1}{\{1+e^{-2\theta(E)}\}}, \tag{3}$$

where $\theta(E)$ is the imaginary action integral evaluated along the reaction coordinate,

$$\theta(E)=\frac{2\pi}{h}\int_{s_l}^{s_r}\sqrt{2\mu_{\mathrm{eff}}(s)|E-V_d(s)|}\,ds \tag{4}$$

and where the integration limits s_l and s_r are the reaction coordinate classical turning points. The reaction-path curvature effect on the tunneling probability is included in the effective reduced mass μ_{eff}. Thus, the ZCT transmission coefficients can be obtained by setting μ_{eff} equal to μ in Eq. (4). Within the centrifugal-dominant small curvature semiclassical tunneling approach,[28] the effective reduced mass is approximated by

$$\mu_{\mathrm{eff}}(s)=\mu\times\min\begin{Bmatrix}\exp\{-2\bar{a}(s)-[\bar{a}(s)]^2+(d\bar{t}/ds)^2\}\\ 1\end{Bmatrix}, \tag{5}$$

where

$$\bar{a}(s)=|\kappa(s)\bar{t}(s)|, \tag{6}$$

and where the effective vibrational turning point $\bar{t}(s)$ in the harmonic approximation is given by

$$\bar{t}(s)=\left(\frac{\kappa\hbar}{\mu}\right)^{1/2}\left\{\sum_{i=1}^{3N-7}[\kappa_i(s)]^2\frac{w_i^2(s)}{(1+2m_i)}\right\}^{-1/4}, \tag{7}$$

and where κ_i is the reaction-path curvature component along mode i in the vibrational state m_i of the reaction-path curvature κ. The reaction-path curvature κ is given by

$$\kappa(s)=\left\{\sum_{i=1}^{3N-7}[B_{iF}]^2\right\}^{1/2}, \tag{8}$$

where B_{iF} is the coupling constant of the vibrational mode i with the reaction coordinate. Note that the larger reaction-path curvature, the smaller the effective reduced mass, and thus it leads to the larger tunneling probability [see Eqs. (5) and (6)]. This fact is important in our later discussion on the differences between the Schatz–Elgersma PEF and our present results. More details on the VTST and CS-SCSAG methods can be found elsewhere.[28–32]

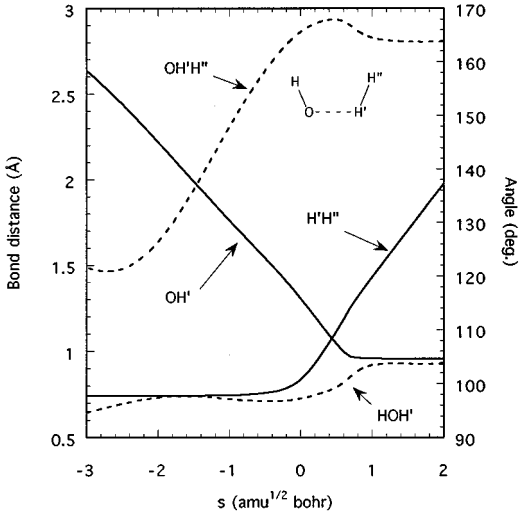

FIG. 1. Geometries along minimum energy path for the $OH+H_2 \leftrightarrow H+H_2O$ reaction plotted vs the reaction coordinate s in the mass-weighted internal coordinates. Solid curves are bond distances (in Å) and dashed curves are angles (in degrees).

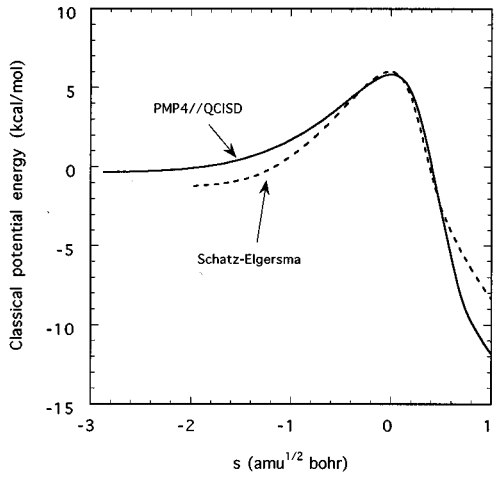

FIG. 2. The classical potential $V_{MEP}(s)$ energy along the MEP as functions of the reaction coordinate s. Solid line is the present PMP4/6-311++G$(2df,2pd)$//QCISD/6-3111+G(d,p) results and dashed line is from the Schatz–Elgersma PEF.

III. COMPUTATIONAL DETAILS

Similar to our previous study,[27] geometries and Hessians along the minimum energy path (MEP) were calculated at the QCISD/6-311+G(d,p) level of theory. The energy along the MEP was further improved by a series of single point PMP4/6-311++G$(2df,2pd)$ calculations at the QCISD/6-311+G(d,p) geometries. The MEP was calculated in the mass-weighted internal coordinates using the second-order Gonzalez and Schlegel method[33] with a step size of 0.01 amu$^{1/2}$ bohr. Note that this step size is a factor of 4 smaller than those used in our previous study and the integration was carried out much further into both the reactant and product sides. The smaller integration step size used in this study was needed to assure accurate B_{iF} dynamical coupling constants in the asymptotic regions. All electronic structure calculations were done by using the GAUSSIAN92 program.[34]

Rate calculations were done using our new DIRATE program.[35] Our previously introduced focusing technique was also used.[27,36,37] However, in this study, we included a total of 83 Hessian points along the MEP including the stationary points to assure convergence in rate constants for all processes considered here, namely the $OH+H_2$, $OH(v=1)+H_2$, and $OH+H_2(v'=1)$ reactions and a continuous description of the vibrational-reaction-coordinate coupling constants B_{iF} as functions of s as discussed below. Other details are the same as in our previous study.[27]

IV. RESULTS AND DISCUSSION

A. Minimum energy path

Geometries along the minimum energy path are shown in Fig. 1 and are similar to our previous study,[27] except that in this study the MEP was integrated much further into both entrance and exit channels, particularly to s equal to -3.0 and 2.0 amu$^{1/2}$ bohr, respectively. Due to a much smaller step size used in this study, the MEP was found to be well behaved even further in the entrance channel.

Classical potential energy along the MEP from the PMP4//QCISD calculations and the Schatz–Elgersma PEF is shown in Fig. 2. Recall from our previous study,[27] we found that single point PMP4 calculations at selected points along the QCISD MEP have shifted the maximum location to the $OH+H_2$ side by 0.13 amu$^{1/2}$ bohr. To obtain more accurate variational effects, we have shifted the origin of the reaction coordinate to the location of the maximum of the PMP4//QCISD potential curve. Note that the barrier heights from both PESs are quite similar. The difference is only by 0.3 kcal/mol. The barrier widths are also remarkably similar particularly for the top half of the barrier, though noticeably narrower width was found for the bottom half of the Schatz–Elgersma PEF. The Schatz–Elgersma PEF has been known to have a complex well with the depth of 1.24 kcal/mol in the entrance channel. The PMP4//QCISD surface also has a well located further out in the entrance channel. The well depth is of only 0.4 kcal/mol and it is consistent with the range of dipole-induced–dipole interaction. It is important to point out that the well in the Schatz–Elgersma PEF has been considered as an artifact and was removed in many dynamical calculations. We found that the PMP4//QCISD PES decreases much faster from the saddle point to the existing $H+H_2O$ channel along the minimum energy path than the Schatz–Elgersma PEF. Consequently, more energy is available for transferring into vibrations in the strong interacting region of the product channel.

The generalized vibrational frequencies as functions of the reaction coordinate are shown in Fig. 3. These frequencies were correlated by maximizing the overlap between normal modes of consecutive Hessian grid points. Our present results are smoother than those from our previous study due to a much finer grid used here. Notice that the QCISD OH and H_2 stretching frequencies are about 200 cm^{-1} larger than

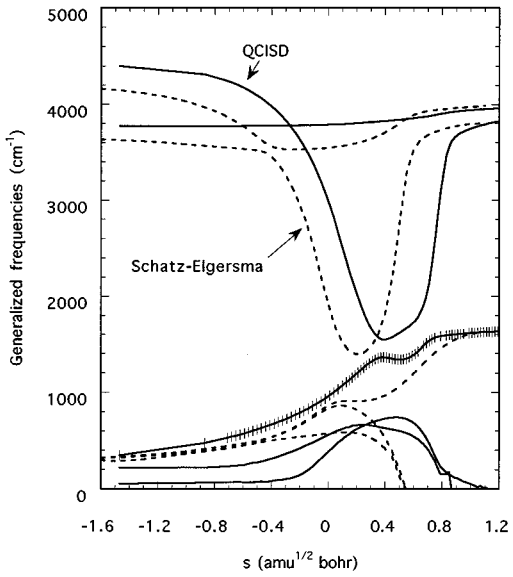

FIG. 3. Harmonic vibrational frequencies along the reaction coordinate s. Solid curves are the QCISD/6-311+G(d,p) results and dashed curves are from the Schatz–Elgersma PEF. Bars are points where QCISD Hessians were calculated.

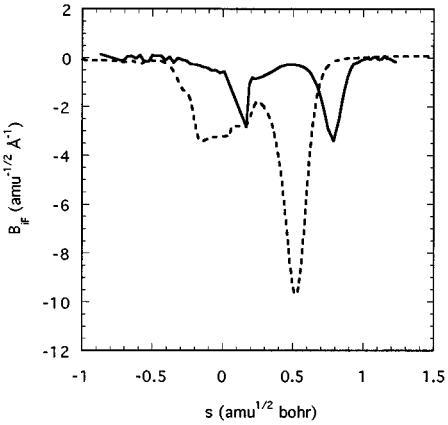

FIG. 4. Vibrational-reaction-coordinate coupling constants B_{iF} for the H_2 stretching mode as functions of the reaction coordinate s. Solid curve is the QCISD/6-311+G(d,p) results and dashed curve is from the Schatz–Elgersma PEF.

those of the Schatz–Elgersma PEF and are more accurate. The QCISD generalized HOH bend is also much larger in the transition state region. An important fact, which has not been discussed in our previous study, is the differences between our *ab initio* results and the Schatz–Elgersma PEF in the behaviors of the two generalized OH and H_2 stretching frequencies. In particular, the QCISD OH and H_2 stretch modes cross at s about -0.35 amu$^{1/2}$ bohr. In the Schatz–Elgersma PEF, these modes approach each other to about 90 cm^{-1} apart in this region but do not cross. In order to get the correct mode specific rate enhancement, Truhlar and Isaacson[9] had introduced a switching function to allow such crossing.

Finally, we examine the B_{iF} dynamical coupling constants for the H_2 stretching mode as functions of the reaction coordinate as shown in Fig. 4. The B_{iF} coupling constants for the OH stretch and HOH bend are quite small relative to those of the H_2 stretch, thus they are not shown in Fig. 4. These coupling constants describe the efficiency of vibrational-to-translational energy transfer in the entrance channel and of translational-to-vibrational energy transfer in the existing channel of a particular vibrational mode as induced by the motion of the reaction coordinate.[38–40] Thus, they can provide useful information for understanding vibrational mode specific rate enhancement. In addition, the B_{iF} constants contribute to the ''corner cutting'' effect in calculating the tunneling probability. Notice that the Schatz–Elgersma PEF predict the B_{iF} couplings for the H_2 stretching mode much larger compared to our QCISD results. This may explain the very large rate enhancement factor for exciting the H_2 stretch obtained in recent full quantum scattering calculations using this PEF. Furthermore, such large B_{iF} couplings also yield a large reaction-path curvature. As a result, it would predict a large corner cutting effect as seen in Truhlar and Isaacson's study.[41] More quantitative discussion on this is given below. It is interesting to also point out that in our *ab initio* calculations the smaller QCISD B_{iF} couplings indicate that the energy release into product vibrations is less efficient but there is much more energy release in the strong interacting region of the product channel as compared to those from the Schatz–Elgersma PEF.

B. Rate constants

The ground-state adiabatic and state-selected diabatic potential energy curves with the zero of energy set at the corresponding reactant values are shown in Fig. 5. Notice that both our *ab initio* calculations and the Schatz–Elgersma PEF yield a similar zero-point energy corrected barrier for the $OH+H_2$ reaction. The distinct difference is that our *ab*

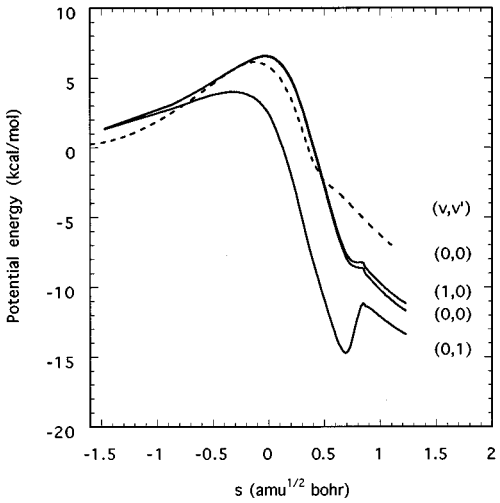

FIG. 5. The vibrational diabatic potential energy curves along the MEP as functions of the reaction coordinate s for the OH(v)+H2(v') reaction with $(v,v')=(0,0)$, (1,0), and (0,1). Solid lines are the present PMP4/6-311++G$(2df,2pd)$//QCISD/6-3111+G(d,p) results and the dashed line for $(v,v')=(0,0)$ is from the Schatz–Elgersma PEF.

TABLE I. Calculated rate constants (cm^3 $molecule^{-1}$ s^{-1}) for the $OH+H_2$, $OH(v=1)+H_2$, and $OH+H_2(v'=1)$ reaction. The notation E-n stands for $\times 10$-n throughout.

	$OH+H_2$			$OH(v=1)+H_2$	$OH+H_2(v'=1)$
T (K)	CVT/ZCT	CVT/SCT	Expt.[a]	CVT/SCT	CVT/SCT
250	1.56E-15	1.64E-15	[1.53E-15][b]	1.55E-15	2.24E-13
300	4.95E-15	5.23E-15	6.18E-15	4.96E-15	4.56E-13
400	3.23E-14	3.36E-14	3.90E-14	3.21E-14	1.46E-12
500	1.18E-13	1.21E-13	1.28E-13	1.17E-13	3.18E-12
600	3.00E-13	3.06E-13	2.98E-13	2.97E-13	5.58E-12
800	1.07E-12	1.08E-12	9.42E-13	1.05E-12	1.21E-11
1000	2.54E-12	2.56E-12	2.04E-12	2.05E-12	2.04E-11
2000	2.10E-11	2.17E-11	1.42E-11	2.14E-11	7.58E-11

[a]Recommended experimental values from Baulch *et al.* (Ref. 42).
[b]Value in the square bracket is extrapolation.

initio PES yields much larger energy release in the strong vibrational-reaction coordinate coupling region in the product side. Exciting the OH stretch yields the diabatic curve nearly identical to the ground-state adiabatic curve and thus is expected to have a negligible effect on the rate. Exciting the H_2 stretch by one quanta significantly reduces the internal vibrational energy corrected barrier from 6.55 to 4.01 kcal/mol and thus is expected to have a large effect on the rate. Thermal and vibrational-state selected rate constants for the $OH+H_2$, $OH(v=1)+H_2$, and $OH+H_2(v=1)$ reactions are listed in Table I. Arrhenius plots of calculated and experimental thermal and state selected rate constants are shown in Figs. 6 and 7, respectively.

1. Thermal rate constants

In this study, thermal rate constants were calculated with a much finer Hessian grid spacing than in our previous study, a total of 83 vs 28 Hessian grid points, respectively. We found that the present rate constants are smaller by at most 22% and in better agreement with the most recently recommended experimental data.[42] Our predicted rate constants are in excellent agreement with experimental data for a relatively wide range of temperatures from 250 to 2000 K. Previous theoretical studies including full quantum[6,11] and CVT/SCSAG[41] calculations based on the Schatz–Elgersma PEF noticeably overestimate rate constants particularly at low temperatures. Such large error has been attributed to the Schatz–Elgersma PEF having narrow potential width. As discussed above, this is not the case. To further clarify this point, we have calculated CVT, CVT/ZCT, and CVT/SCT rate constants using the Schatz–Elgersma PEF and compared to results from our *ab initio* calculations. Recall that SCT denotes the CD-SCSAG tunneling method which was found to yield more accurate tunneling probability than the SCSAG method used in a previous Truhlar and Isaacson study.[41] Since the same dynamical method was used, the differences in the rate constants must originate from the inherent differences in the PES used. At 300 K, both *ab initio* and Schatz–

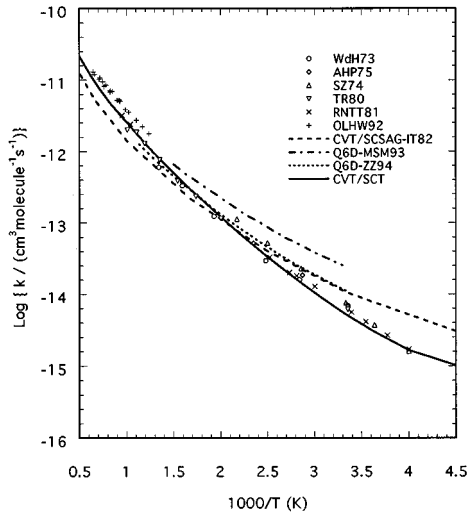

FIG. 6. Arrhenius plot of the $OH+H_2$ rate constants vs $1/T$. The solid line is the present CVT/SCT results. The short dashed line is from previous CVT/SCSAG results (Ref. 41). Dashed–dotted and dotted lines are from full quantum calculations (Refs. 6 and 11, respectively). WdH73, Ref. 20; AHP75, Ref. 21; SZ74, Ref. 19; TR80, Ref. 22; RNTT81, Ref. 18; OLHW92, Ref. 23.

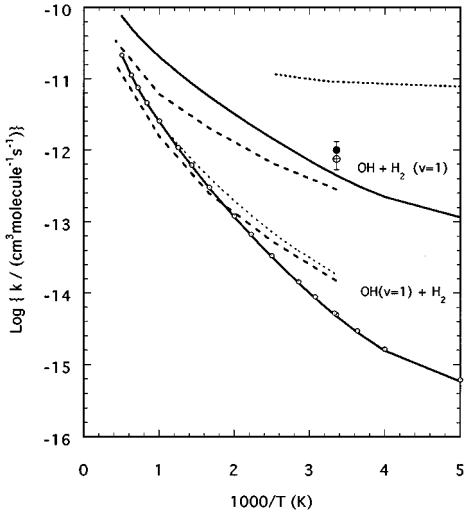

FIG. 7. Arrhenius plot of the $OH(v=1)+H_2$ (lower curves) and $OH+H_2(v=1)$ (upper curves) rate constants vs $1/T$. The solid lines are the present CVT/SCT results. The dashed lines are from previous CVT/SCSD results (Ref. 9). Dotted lines are from full quantum calculation (Ref. 11). Filled and opened circles are experimental data (Refs. 24 and 25, respectively).

TABLE II. Calculated and experimental rate enhancement factors at 298 K for the $OH(v=1)+H_2$ and $OH+H_2(v'=1)$ reactions.

	$OH(v=1)+H_2$	$OH+H_2(v'=1)$
Experimental	<1.6[a]	120 ± 40[b], 155 ± 38[c]
Theoretical		
CVT/SCSD[d]	1.42	26.9
QCT (300 K)[e]	1.28	393
RBA[f]		154
Full quantum (300 K)[g]	1.69	805
This work		
TST/W	0.90	20 020
CVT	0.93	180
CVT/ZCT	0.95	93.6
CVT/SCT[h]	0.95	88.7

[a]Reference 26.
[b]Reference 25.
[c]Reference 24.
[d]Reference 9.
[e]Reference 10.
[f]Reference 1.
[g]Reference 11.
[h]Our best results.

Elgersma PESs yield nearly identical CVT rate constants and ZCT transmission coefficients with differences by less than 8%. CVT rate constants are more sensitive to the barrier height whereas the ZCT tunneling transmission coefficients are more sensitive to the barrier width, i.e., the larger barrier width yields the longer tunneling path and as results the smaller ZCT tunneling probability. These results confirm our earlier discussion that the barrier and the potential width of both PESs are nearly the same. Including the reaction-path curvature effect in calculating the tunneling probability within the SCT approximation enhances the rate by a factor of 2.66 at 300 K using the Schatz–Elgersma PEF, and only a factor of 1.05 using our *ab initio* PES. This further confirms our earlier finding that the reaction-path curvature of the Schatz–Elgersma PEF is too large. This also explains the large calculated kinetic isotope effects (k_{H_2}/k_{D_2}) using the Schatz–Elgersma PEF, particular at low temperatures.[41]

2. $OH(v=1)+H_2$ reaction

CVT/SCT rate constants for the $OH(v=1)+H_2$ reaction, where H_2 vibration is treated thermally, are slightly smaller than our calculated thermal rate and are plotted in Fig. 7. At the temperature of 298 K, the difference is of a factor of 0.95 which is consistent with experimental observation (see Table II).[26] However, all previous calculations using the Schatz–Elgersma PEF predicted a small enhancement factor ranging from 1.28 to 1.69 at 298 K. The differences can be understood by examining the generalized frequency plot shown in Fig. 3. The changes in the QCISD OH frequency from the reactant to the transition state are slightly positive. Thus, exciting the OH mode would raise the effective barrier slightly. The opposite is observed for the Schatz–Elgersma PEF after making the diabatic approximation. Note that in QCT and quantum scattering calculations, the H_2 vibrational mode is often restricted to the ground state. We found that restricting H_2 vibration to the ground state only yields at most 5% difference in the calculated rate constants for the $OH(v=1)+H_2$ reaction.

3. $OH+H_2(v'=1)$ reaction

The predicted rate constants for the $OH+H_2(v'=1)$ reaction are also listed in Table I and are plotted vs the temperature in Fig. 7 along with experimental data[24,25] and results from previous theoretical studies.[9,11] In the present study, the OH vibration was treated thermally, though we also found that restricting the OH vibration in the ground state only yields negligible differences in the rate. Figure 7 shows that our predicted rate constants for the $OH+H_2(v'=1)$ reaction are in excellent agreement with experimental data, though slightly too low. Our predicted enhancement factors ranging from 180 to 88.7 at various levels of theory, namely CVT, CVT/ZCT, and CVT/SCT, listed in Table II are within the experimental uncertainty that ranges from 80 to 193.[24,25] It has been known that the conventional transition state theory plus Wigner tunneling correction (TST/W) significantly overestimates the enhancement factor. This is due to the reason as pointed out in Truhlar and Isaacson's study[9] that the dynamical bottlenecks for the $OH+H_2(v'=1)$ are shifted significantly away from the saddle point toward the reactants.

Our present results are particularly encouraging since using a direct *ab initio* dynamics method we were not only able to predict accurate thermal rate constants and kinetic isotope effects of the $OH+H_2 \leftrightarrow H+H_2O$ reaction as shown in our recent study,[27] but also vibrational-state selected rate for exciting either the OH or H_2 stretching mode from first principles.

V. CONCLUSIONS

We have performed direct *ab initio* dynamics studies of vibrational-state selected rates of the $OH(v)+H_2(v') \rightarrow H+H_2O$ reaction. These calculations were based on a full variational transition state theory plus multidimensional semiclassical tunneling corrections within a diabatic model where vibrational modes are assumed to preserve their characteristics along the reaction coordinate. The potential energy information was calculated at an accurate level of *ab initio* molecular orbital theory. In particular, geometries and frequencies along the minimum energy path and at the reactants and products were calculated at the QCISD/6-311 $+G(d,p)$ level. Energetic information was further improved at the PMP4/6-311++G$(2df,2pd)$ level.

We found that the calculated thermal and state selected rate constants for the $OH+H_2$, $OH(v=1)+H_2$, and $OH+H_2(v'=1)$ reactions are in excellent agreement with available experimental data. In particular, our predicted rate enhancement factors due excitations of either the reagent OH or H_2 stretching mode are within the experimental uncertainties whereas previous theoretical predictions were either too high or too low for the $OH+H_2(v'=1)$ reaction. This is particularly encouraging since applications of our direct *ab initio* dynamics methodology to larger polyatomic reactions are straightforward whereas conventional dynamical approach is

limited to the availability of accurate analytical potential force field and also to the size of the system in the case of full quantum consideration. Our present results also illustrate the sensitivity of dynamical results on the quality of the analytical potential energy function used. In particular, we found that even though the Schatz–Elgersma PEF has similar barrier height and width with our *ab initio* PES, the large vibrational-reaction coordinate, B_{iF}, coupling constants in the Schatz–Elgersma PEF lead to significant overestimation of tunneling contributions at low temperatures and may also contribute to the significantly large enhancement factor for the $OH+H_2(v'=1)$ reaction predicted by full quantum scattering calculations. Such aspects of the PEF have not often been examined in the past.

ACKNOWLEDGMENTS

This work was supported in part by the National Science Foundation through a Young Investigator Award. The author also thank the Utah Supercomputing Institute for computer time.

[1] D. C. Clary, J. Chem. Phys. **96**, 3656 (1992).
[2] D. C. Clary, J. Chem. Phys. **95**, 7298 (1991).
[3] J. A. Harrison and H. R. Mayne, J. Chem. Phys. **88**, 7424 (1988).
[4] G. C. Schatz and H. Elgersma, Chem. Phys. Lett. **73**, 21 (1980).
[5] D. Wang and J. M. Bowman, J. Chem. Phys. **96**, 8906 (1992).
[6] U. Manthe, T. Seideman, and W. H. Miller, J. Chem. Phys. **99**, 10,078 (1993).
[7] D. H. Zhang and J. Z. H. Zhang, J. Chem. Phys. **99**, 5615 (1993).
[8] K. S. Bradley and G. C. Schatz, J. Phys. Chem. **98**, 3788 (1994).
[9] D. G. Truhlar and A. D. Isaacson, J. Chem. Phys. **77**, 3516 (1982).
[10] G. C. Schatz, J. Chem. Phys. **74**, 1133 (1981).
[11] D. H. Zhang and J. Z. H. Zhang, J. Chem. Phys. **101**, 1146 (1994).
[12] D. Neuhauser, J. Chem. Phys. **101**, 9272 (1994).
[13] H. Szichman and M. Baer, J. Chem. Phys. **101**, 2081 (1994).
[14] N. Balakrishnan and G. D. Billing, J. Chem. Phys. **101**, 2785 (1994).
[15] J. Echave and D. C. Clary, J. Chem. Phys. **100**, 402 (1994).
[16] J. R. Fisher and J. V. Michael, J. Phys. Chem. **90**, 2465 (1990).
[17] J. V. Michael and J. W. Sutherland, J. Phys. Chem. **92**, 3853 (1988).
[18] A. R. Ravishankara, J. M. Nicovich, R. L. Thompson, and F. P. Tully, J. Phys. Chem. **85**, 2498 (1981).
[19] I. W. M. Smith and R. Zellner, J. Chem. Soc. Faraday Trans. 2 **70**, 2290 (1974).
[20] A. A. Westenberg and N. deHass, J. Chem. Phys. **58**, 4061 (1973).
[21] R. Atkinson, D. A. Hansen, and J. Pitts J. N., J. Chem. Phys. **63**, 1703 (1975).
[22] F. P. Tully and A. R. Ravishankara, J. Phys. Chem. **84**, 3126 (1980).
[23] R. C. Oldenborg, G. W. Loge, D. M. Harradine, and K. R. Winn, J. Phys. Chem. **96**, 8426 (1992).
[24] G. P. Glass and B. K. Chaturvedi, J. Chem. Phys. **75**, 2749 (1981).
[25] R. Zellner and W. Steinert, Chem. Phys. Lett. **81**, 568 (1981).
[26] J. E. Spencer, H. Endo, and G. P. Glass, in *Proceedings of the 16th Symposium (Int.) Combustion* (Combustion Institute, Pittsburgh, 1977), p. 829.
[27] T. N. Truong and T. J. Evans, J. Phys. Chem. **98**, 9558 (1994).
[28] D.-h. Lu, T. N. Truong, V. S. Melissas, G. C. Lynch, Y. P. Liu, B. C. Garrett, R. Steckler, A. D. Isaacson, S. N. Rai, G. C. Hancock, J. G. Lauderdale, T. Joseph, and D. G. Truhlar, Comput. Phys. Commun. **71**, 235 (1992).
[29] S. C. Tucker and D. G. Truhlar, in *New Theoretical Concepts for Understanding Organic Reactions*, edited by J. Bertran and I. G. Csizmadia (Kluwer, Dordrecht, 1989), pp. 291–346.
[30] D. G. Truhlar, A. D. Isaacson, R. T. Skodje, and B. C. Garrett, J. Phys. Chem. **86**, 2252 (1982).
[31] D. G. Truhlar, A. D. Isaacson, and B. C. Garrett, in *Theory of Chemical Reaction Dynamics*, edited by M. Baer (Chemical Rubber, Boca Raton, 1985), Vol. 4, pp. 65–137.
[32] D. G. Truhlar and B. C. Garrett, Annu. Rev. Phys. Chem. **35**, 159 (1984).
[33] C. Gonzalez and H. B. Schlegel, J. Phys. Chem. **94**, 5523 (1990).
[34] M. J. Frisch, G. W. Trucks, M. Head-Gordon, P. M. W. Gill, M. W. Wong, J. B. Foresman, B. G. Johnson, H. B. Schlegel, M. A. Robb, E. S. Replogle, R. Gomperts, J. L. Andres, K. Raghavachari, J. S. Binkley, C. Gonzalez, R. L. Martin, D. J. Fox, D. J. Defrees, J. Baker, J. J. P. Stewart, and J. A. Pople, GAUSSIAN92 (Gaussian, Pittsburgh, PA, 1992).
[35] T. N. Truong, *DiRate* (University of Utah, Salt Lake City, 1993) (unpublished).
[36] T. N. Truong, J. Chem. Phys. **100**, 8014 (1994).
[37] T. N. Truong and W. T. Duncan, J. Chem. Phys. **101**, 7408 (1994).
[38] E. Kraka and T. H. Dunning, Jr., in *Advances in Molecular Electronic Structure Theory*, edited by T. H. Dunning, Jr. (JAI, Greenwich, 1990), Vol. 1, p. 129.
[39] T. H. Dunning, R. A. Eades, and E. Kraka, Faraday Discuss. Chem. Soc. **1987**, 427.
[40] T. H. Dunning, J. M. Bowman, G. C. Schatz, A. F. Wagner, and L. B. Harding, Science **240**, 453 (1988).
[41] A. D. Isaacson and D. G. Truhlar, J. Chem. Phys. **76**, 1380 (1982).
[42] D. L. Baulch, C. J. Cobos, R. A. Cox, C. Esser, P. Frank, T. Just, J. A. Kerr, M. J. Pilling, J. Troe, R. W. Walker, and J. Warnatz, J. Phys. Chem. Ref. Data **21**, 441 (1992).